Electronic Supplementary Material (ESI) for Dalton Transactions.


# AlP-regulated phosphorus vacancies over Ni-P compounds promoting efficient and durable hydrogen generation in acidic media

Mei Wang,*[a] Huifang Zhao,[a] Yi Long,[a] Wenjuan Zhang,[c] Liyong Wang,[a] Diaoyu Zhou,[a] Huiqi Wang*[a] and Xiaoguang Wang*[b]

[a] School of Materials Science and Engineering & School of Energy and Power Engineering & School of Science, North University of China, Taiyuan 030051, China. E-mail: wangmei@nuc.edu.cn, hqiwang@nuc.edu.cn

[b] Laboratory of Advanced Materials and Energy Electrochemistry, School of Materials Science and Engineering, Taiyuan University of Technology, Taiyuan 030024, China. E-mail: wangxiaog1982@163.com

[c] Department de Química, Universitat Autònoma de Barcelona (UAB), 08193 Bellaterra (Cerdanyola del Vallès), Spain

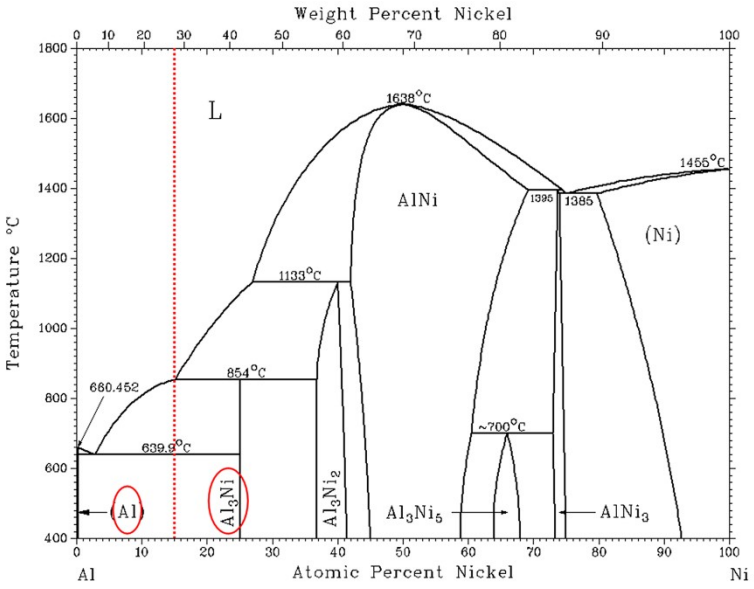


**Fig. S1** The binary phase diagram of $Al_{85}Ni_{15}$.

In Fig. S1, the red dash line indicates the nominal composition (at. %) of $Al_{85}Ni_{15}$ alloy ingot, producing Al phase and $Al_3Ni$ phase after rapid cooling.

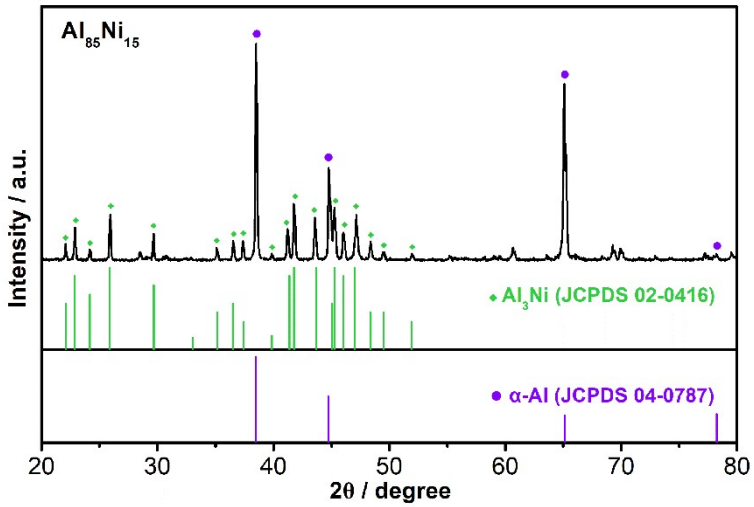


**Fig. S2** XRD pattern of $Al_{85}Ni_{15}$ electrode

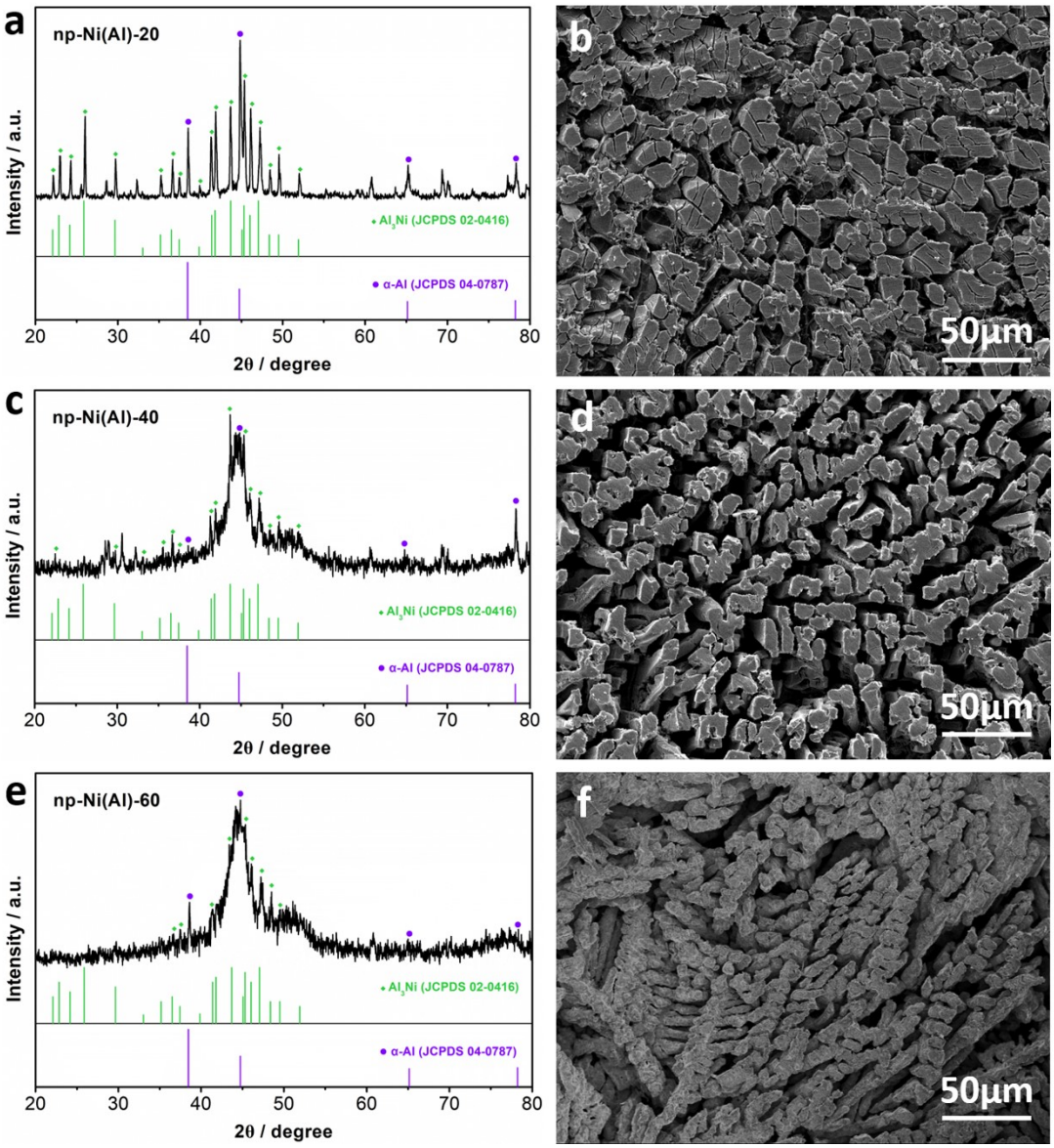


**Fig. S3** XRD patterns of (a) np-Ni(Al)-20, (c) np-Ni(Al)-40 and (e) np-Ni(Al)-60 electrodes. SEM images of (b) np-Ni(Al)-20, (d) np-Ni(Al)-40 and (f) np-Ni(Al)-60 electrodes.

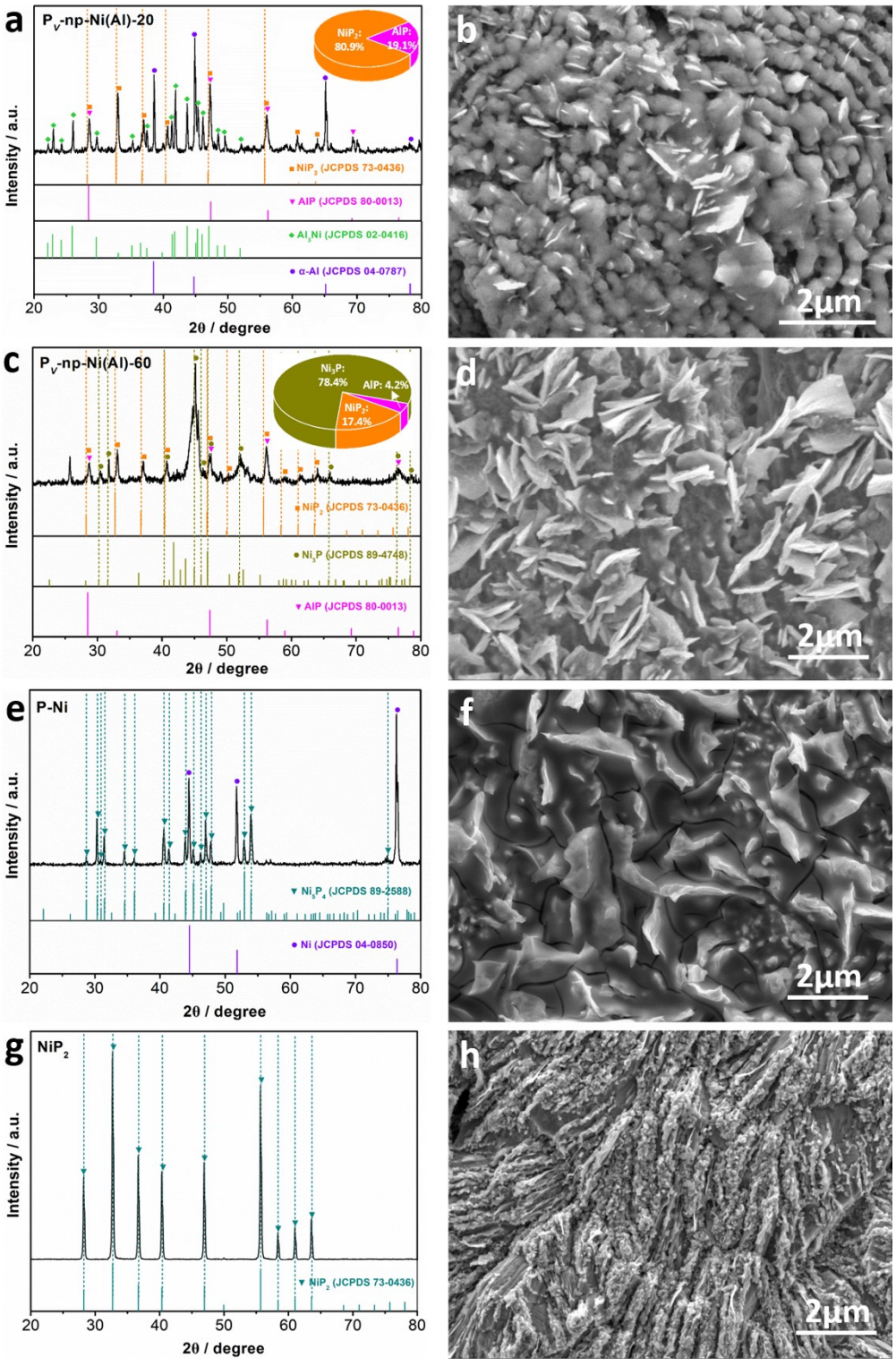


**Fig. S4** XRD patterns and quantitative phase composition analysis of (a) $P_V$-np-Ni(Al)-20, (c) $P_V$-np-Ni(Al)-60, (e) P-Ni and (g) $NiP_2$ electrodes. SEM images of (b) $P_V$-np-Ni(Al)-20, (d) $P_V$-np-Ni(Al)-60, (f) P-Ni and (h) $NiP_2$ electrodes.

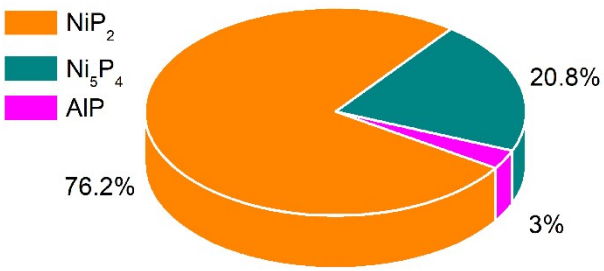


**Fig. S5** The quantitative phase composition analysis of $P_V$-np-Ni(Al)-40.

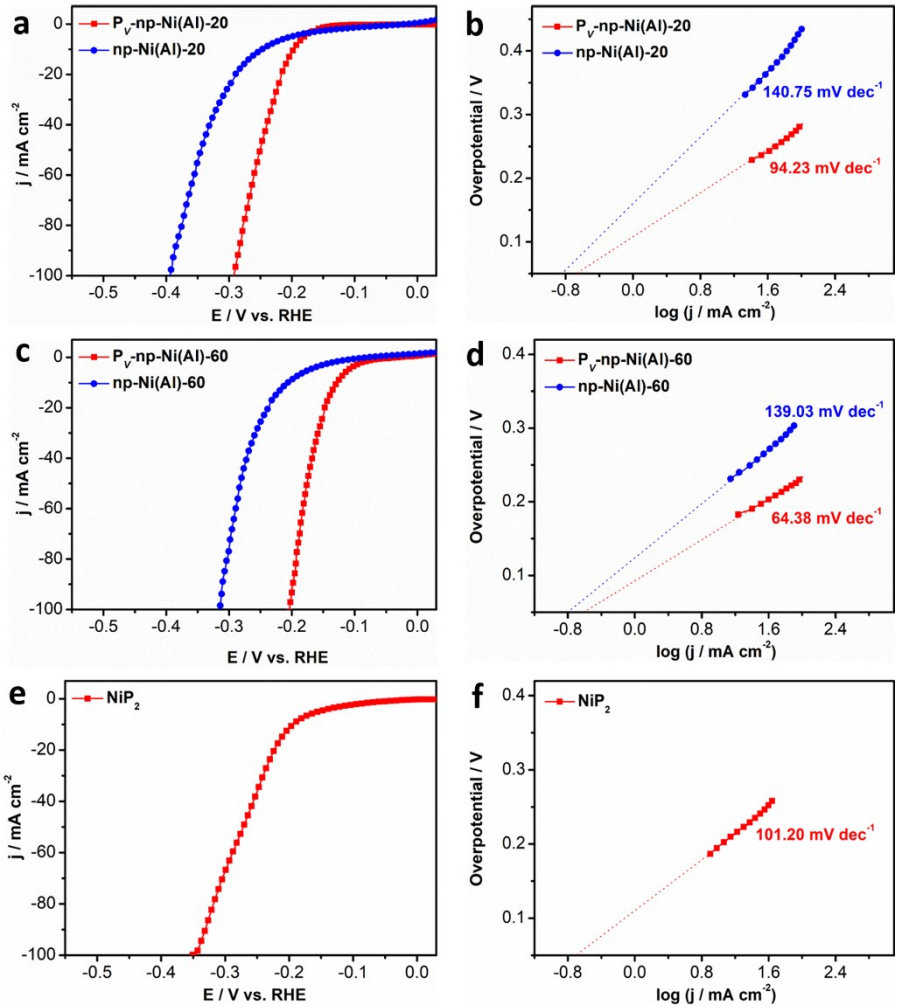


**Fig. S6** (a) Polarization curves and (b) Tafel plots of $P_V$-np-Ni(Al)-20 and np-Ni(Al)-20 electrocatalysts; (c) Polarization curves and (d) Tafel plots of $P_V$-np-Ni(Al)-60 and np-Ni(Al)-60 electrocatalysts; (e) Polarization curves and (f) Tafel plots of $NiP_2$ electrocatalyst.

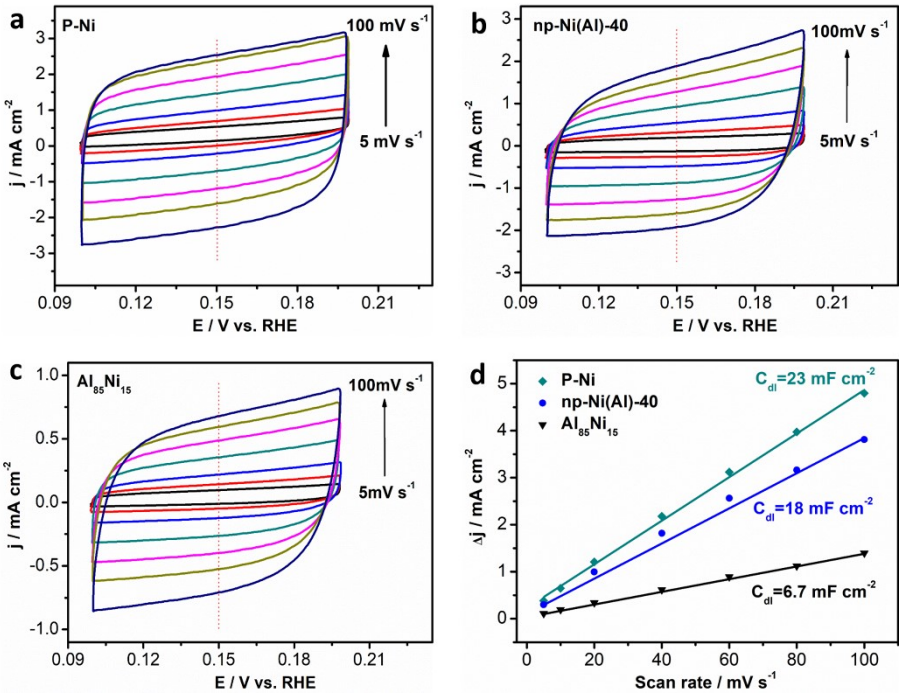


**Fig. S7** CV curves (0.1～0.2 V vs. RHE) of (a) P-Ni, (b) np-Ni(Al)-40 and (c) $Al_{85}Ni_{15}$ electrodes under different scan rates. (c) The capacitive currents at the middle of potential window as a function of scan rate.

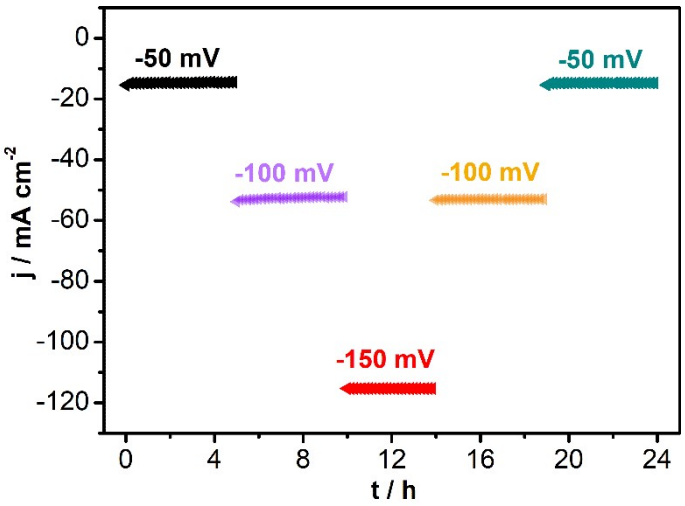


**Fig. S8** Chronoamperometric curves of $P_V$-np-Ni(Al)-40 measured at different overpotentials.

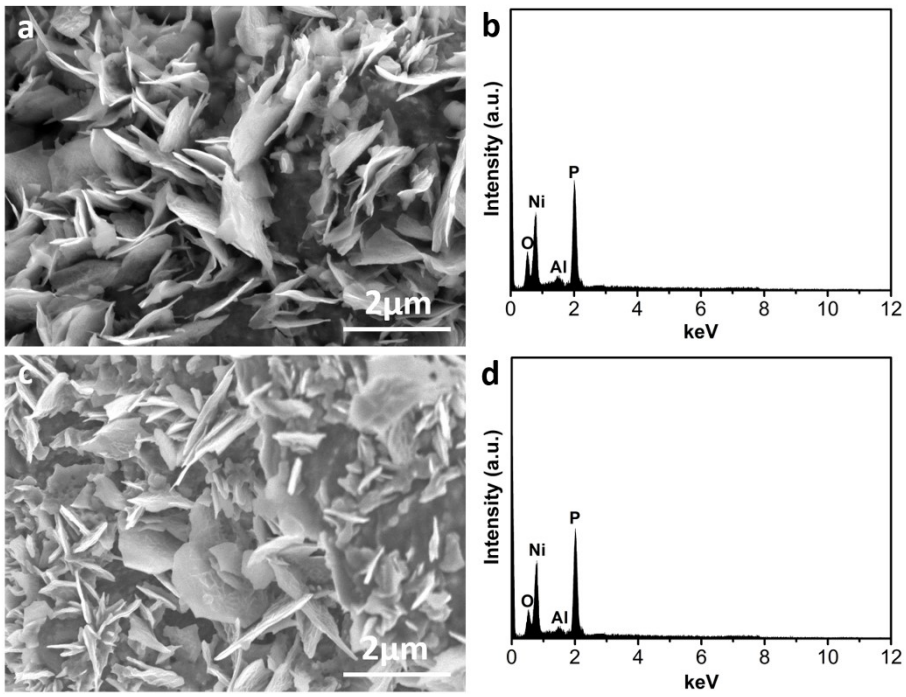


**Fig. S9** (a, c) SEM images of $P_V$-np-Ni(Al)-40 electrode before and after both accelerated degradation test for 5000 continuous cycles and subsequent chronopotentiometric test at a constant cathodic current of 10 mA $cm^{-2}$ for 96 h in 0.5 M $H_2SO_4$ solution. (b, d) The corresponding EDX spectrums.

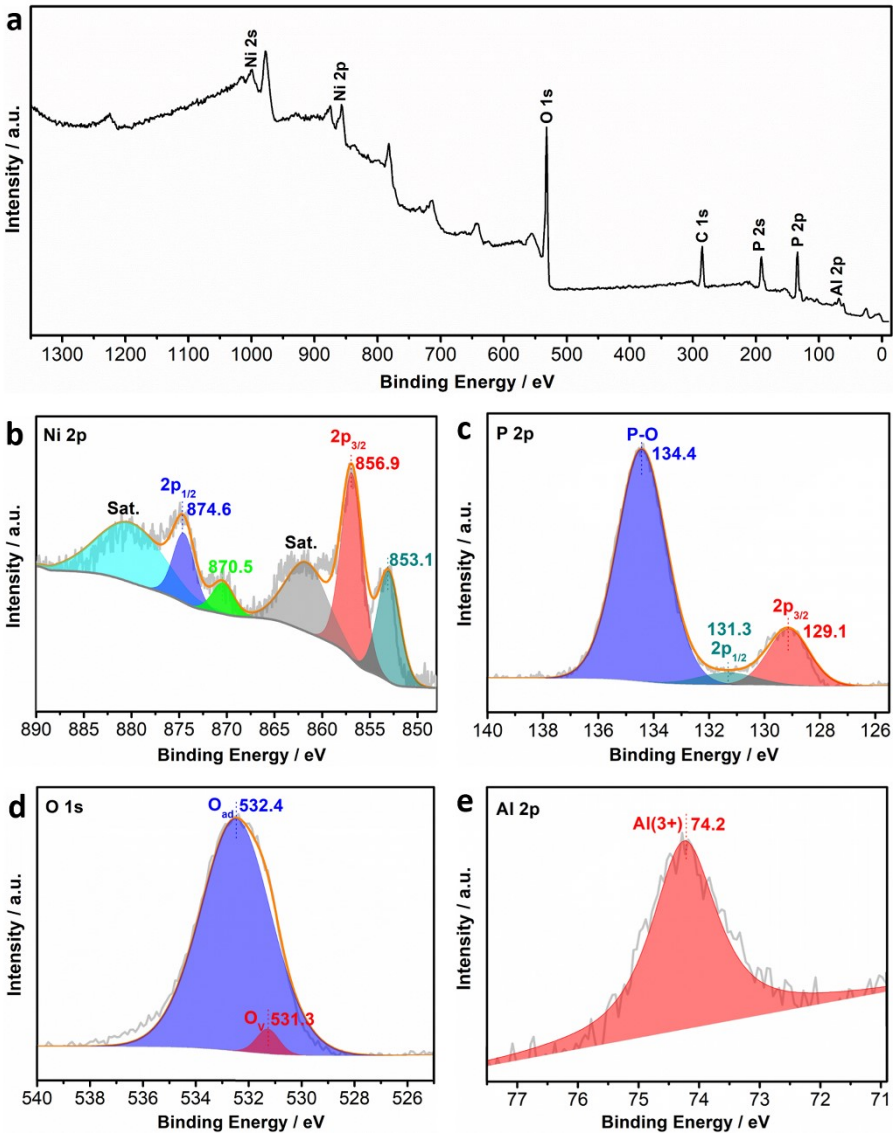


**Fig. S10** XPS spectra of $P_V$-np-Ni(Al)-40 electrode after HER tests: (a) Survey scan; (b) Ni 2p; (c) P 2p; (d) O 1s; (e) Al 2p.

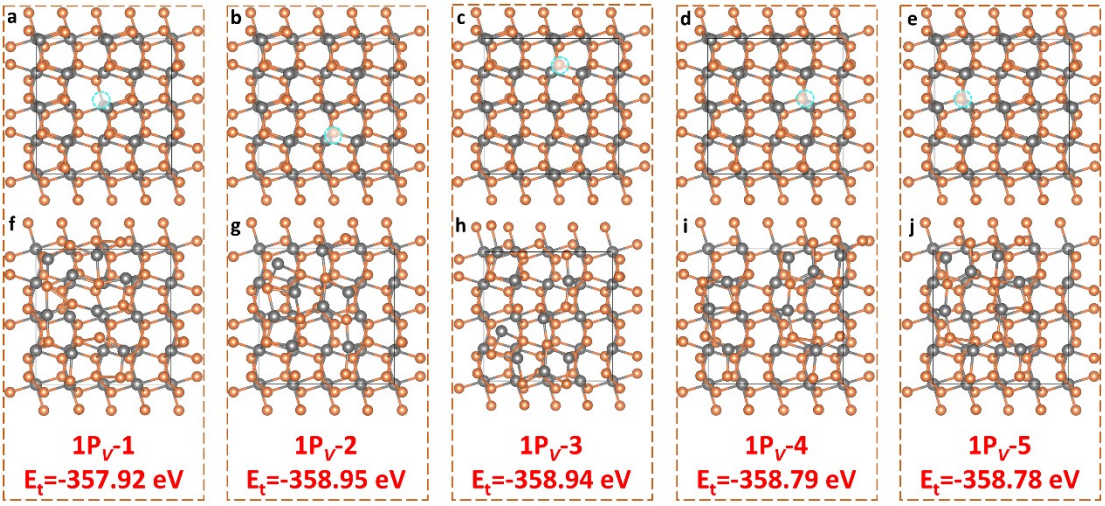


**Fig. S11** (a-e) The slab models of $1P_V$-$NiP_2$ with different $P_V$ site; (f-j) The optimized models and corresponding total energies of $1P_V$-$NiP_2$ with different $P_V$ site.

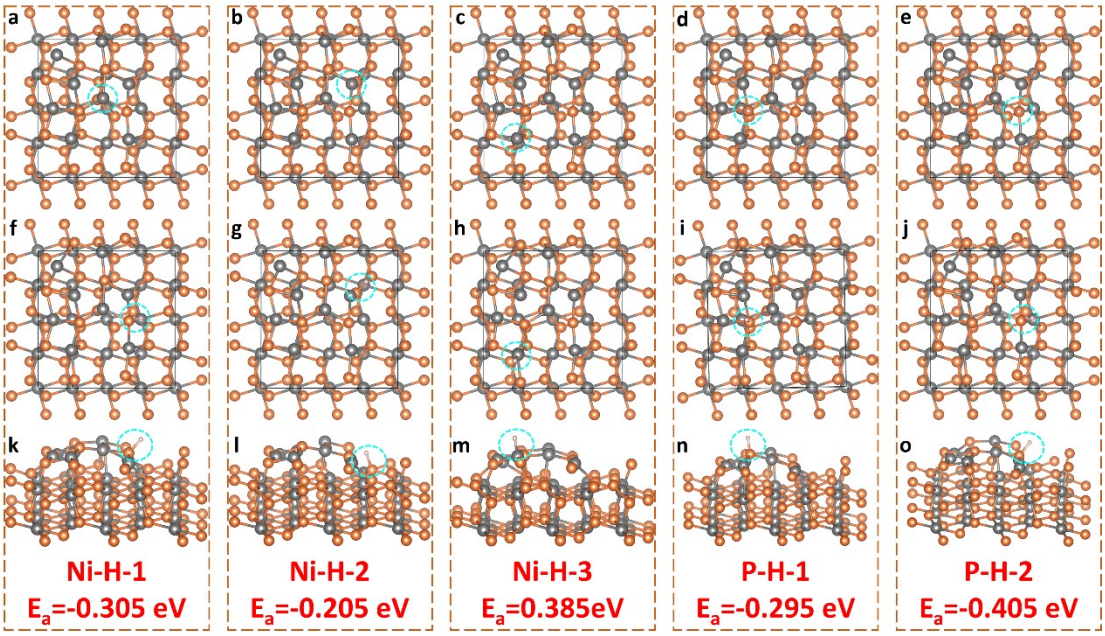


**Fig. S12** H* adsorption models of $1P_V$-$NiP_2$ on different (a-c) Ni sites and (d, e) P sites; (f-j) Top view of optimized H* adsorption models; (k-o) Side view and corresponding adsorption energies of optimized H* adsorption models.

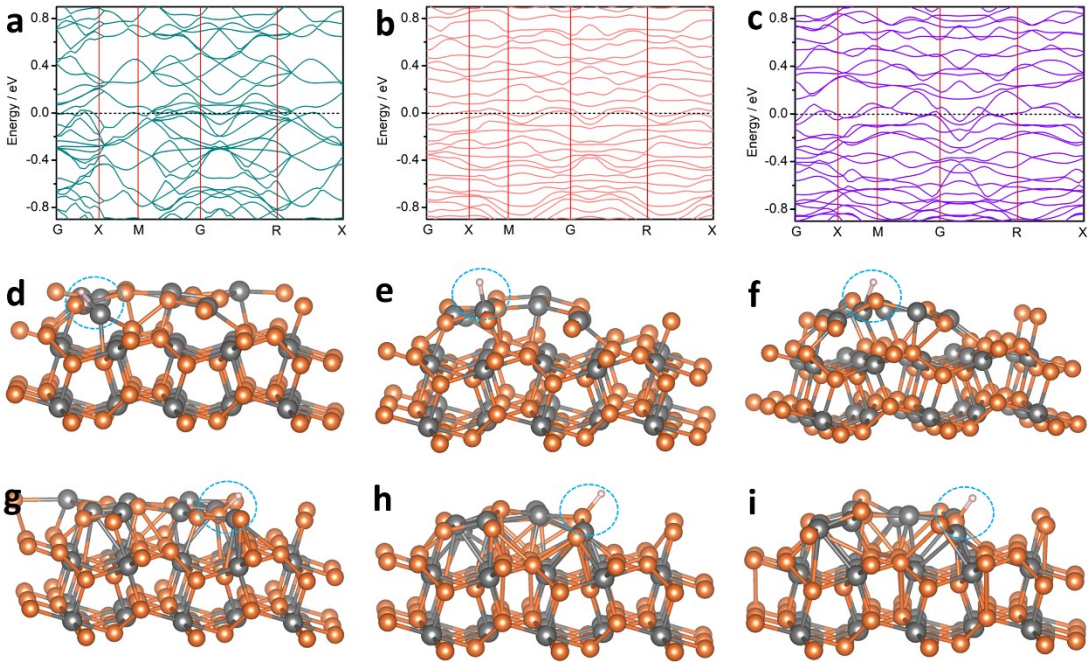


**Fig. S13** Electronic band structures of (a) $NiP_2$; (b) $1P_V$-$NiP_2$; (c) $2P_V$-$NiP_2$. Schematic models of optimized (d) $NiP_2$; (e) $1P_V$-$NiP_2$; (f) $2P_V$-$NiP_2$ with H* adsorbed on their Ni sites. Schematic models of optimized (g) $NiP_2$; (h) $1P_V$-$NiP_2$; (i) $2P_V$-$NiP_2$ with H* adsorbed on their P sites.

**Supplementary Note 1: Turnover frequency (TOF) calculations**

The TOF can be calculated with the following equation:[1]

$$TOF = \frac{number\ of\ total\ hydrogen\ turnovers\ per\ cm^2}{number\ of\ active\ sites\ per\ cm^2} \quad (1)$$

The total number of hydrogen turnovers is calculated from the current density extracted from the LSV curve according to:[2]

$$NO.\ of\ H_2 = \left(|j|\frac{mA}{cm^2}\right)\left(\frac{1\ C\ s^{-1}}{1000\ mA}\right)\left(\frac{1\ mol\ e^{-1}}{96485.3\ C}\right)\left(\frac{1\ mol\ H_2}{2\ mol\ e^{-1}}\right)\left(\frac{6.022 \times 10^{23}\ H_2}{1\ mol}\right.$$

$$= 3.12 \times 10^{15}\ \frac{H_2/s}{cm^2}\ per\ \frac{mA}{cm^2} \quad (2)$$

Since the exact hydrogen binding site is not known, we estimate the number of active sites from the roughness factor together with the unit cell (volume = 163.72 Å$^3$) of $NiP_2$ crystal structure. Hence, the number of active sites per real surface area is calculated according to the crystal data as follows:

$$NO.\ of\ active\ sites = \left(\frac{4\ atom/unit\ cell}{0.16372\ nm^3/unit\ cell}\right)^{2/3} = 8.42 \times 10^{14}\ atoms\ per\ cm^2 \quad (3)$$

Finally, the plot of current density can be converted into a TOF plot according to:

$$TOF = \frac{\left(3.12 \times 10^{15}\ \frac{H_2/s}{cm^2}\ per\ \frac{mA}{cm^2}\right) \times |j|}{\left(8.42 \times 10^{14}\ atoms\ per\ cm^2\right) \times ECSA} = 3.8 \times 10^{-3} \times |j|$$

(4)

**Table S1.** Comparison of HER performance in acid medium for all the as-prepared catalysts in this study.

| Catalysts | $\eta_{onset}$ (mV) | $\eta_{10}$ (mV) | $\eta_{100}$ (mV) | Tafel slope (mV $dec^{-1}$) | $j_0$ (mA $cm^{-2}$) |
|---|---|---|---|---|---|
| $Al_{85}Ni_{15}$ | 123 | 274 | -- | 145.70 | 0.127 |
| np-Ni(Al)-20 | 77 | 247 | 394 | 140.75 | 0.145 |
| $P_V$-np-Ni(Al)-20 | 145 | 197 | 292 | 94.23 | 0.214 |
| np-Ni(Al)-40 | 38 | 168 | 324 | 131.77 | 0.202 |
| **$P_V$-np-Ni(Al)-40** | **11** | **36** | **139** | **38.03** | **0.542** |
| np-Ni(Al)-60 | 113 | 206 | 313 | 139.03 | 0.159 |
| $P_V$-np-Ni(Al)-60 | 71 | 128 | 204 | 64.38 | 0.254 |
| P-Ni ($Ni_5P_4$) | 37 | 90 | 221 | 60.34 | 0.302 |
| $NiP_2$ | 55 | 195 | 351 | 101.20 | 0.196 |
| Pt/C | 11 | 44 | 109 | 31.81 | 0.564 |

**Table S2.** Comparison of HER performance in acid medium for P-np-Ni(Al)-40 with other reported catalysts.

| Catalysts | $\eta_{10}$ (mV) | Tafel slope (mV $dec^{-1}$) | Reference |
|---|---|---|---|
| FeP nanosheet/Ti | 79 | 58 | [3] |
| $FeP_2$-$NiP_2$@PC | 117 | 47 | [4] |
| Ni-MoP | 102 | 58.1 | [5] |
| A-MoP@PC | 68 | 41 | [6] |
| $FeCoP_2$@NPPC | 114 | 79 | [7] |
| NPSCL@S-MoP NSs/CC | 65 | 49.5 | [8] |
| $Rh_2P$/NPC | 40 | 33 | [9] |
| CoP/CN/Ni | 66 | 39.5 | [10] |
| CoP-InNC@CNT | 153 | 62 | [11] |
| P-$Ti_3C_2T_x$@NiCoP | 115 | 76 | [12] |
| **$P_V$-np-Ni(Al)-40** | **36** | **56.58** | **This work** |

**Table S3.** Electrochemical impedance parameters obtained by fitting the Nyquist plots of $P_V$-np-Ni(Al)-40, P-Ni, np-Ni(Al)-40 and $Al_{85}Ni_{15}$ to the equivalent circuit model.

| Catalysts | $R_s$ (Ω) | $R_{ct}$ (Ω) | $Q_1$ (F $cm^{-2}$) | $n_1$ |
|---|---|---|---|---|
| $P_V$-np-Ni(Al)-40 | 0.393 | 5.019 | 0.0191 | 0.826 |
| P-Ni | 1.632 | 7.332 | 0.0051 | 0.865 |
| np-Ni(Al)-40 | 1.036 | 19.79 | 0.0225 | 0.829 |
| $Al_{85}Ni_{15}$ | 1.491 | 21.89 | 0.0129 | 0.913 |

**Table S4.** The atomic ratio of Ni 2p and P 2p peaks for $P_V$-np-Ni(Al)-40 electrode before and after HER test.

| Catalyst | Ni 2p (%) | | | | P 2p (%) | | |
|---|---|---|---|---|---|---|---|
| | $Ni^{\delta+}$ | $Ni^{2+}$ | Sat. | Sum | $P^{\delta-}$ | $P^{5+}$ | Sum |
| Pristine $P_V$-np-Ni(Al)-40 | 4.06 | 58.90 | 37.04 | 100 | 17.03 | 82.97 | 100 |
| Post-tested $P_V$-np-Ni(Al)-40 | 19.11 | 40.27 | 40.63 | 100 | 21.09 | 78.91 | 100 |

**Table S5.** Average Bader charge difference of $NiP_2$, $1P_V$-$NiP_2$ and $2P_V$-$NiP_2$.

| Electrode | $NiP_2$ | | $1P_V$-$NiP_2$ | | $2P_V$-$NiP_2$ | |
|---|---|---|---|---|---|---|
| Element | Ni | P | Ni | P | Ni | P |
| $Q_{total}$/e | 9.904 | 5.057 | 9.894 | 5.067 | 9.886 | 5.07 |
| ΔQ/e | -0.096 | 0.057 | -0.106 | 0.067 | -0.114 | **0.07** |

1 H. Fei, J. Dong, M. J. Arellano-Jimenez, G. Ye, N. Dong Kim, E. L. Samuel, Z. Peng, Z. Zhu, F. Qin, J. Bao, M. J. Yacaman, P. M. Ajayan, D. Chen and J. M. Tour, *Nat. Commun.,* 2015, **6**, 8668.

2 J. Kibsgaard and T. F. Jaramillo, *Angew. Chem. Int. Ed.,* 2014, **53**, 14433-14437.

3 X. Zhao, Z. Zhang, X. Cao, J. Hu, X. Wu, A. Y. R. Ng, G.-P. Lu and Z. Chen, *Appl. Catal. B,* 2020, **260**, 118156.

4 P. Ji, H. Jin, H. Xia, X. Luo, J. Zhu, Z. Pu and S. Mu, *ACS Appl. Mater. Interfaces,* 2019, **12**, 727-733.

5 W. Xiao, L. Zhang, D. Bukhvalov, Z. Chen, Z. Zou, L. Shang, X. Yang, D. Yan, F. Han and T. Zhang, *Nano Energy,* 2020, **70**, 104445.

6 H. Jiang, L. Yan, S. Zhang, Y. Zhao, X. Yang, Y. Wang, J. Shen, X. Zhao and L. Wang, *Nano-Micro Lett.,* 2021, **13**, 215.

7 Y. N. Wang, Z. J. Yang, D. H. Yang, L. Zhao, X. R. Shi, G. Yang and B. H. Han, *ACS Appl. Mater. Interfaces,* 2021, **13**, 8832-8843.

8 H. Li, M. Hu, B. Cao, P. Jing, B. Liu, R. Gao, J. Zhang, X. Shi and Y. Du, *Small,* 2021, **17**, 2006617.

9 S. Liu, Y. Chen, L. Yu, Y. Lin, Z. Liu, M. Wang, Y. Chen, C. Zhang, Y. Pan, Y. Liu and C. Liu, *J. Mater. Chem. A,* 2020, **8**, 25768-25779.

10 T. Chen, J. Ma, S. Chen, Y. Wei, C. Deng, J. Chen, J. Hu and W. Ding, *Chem. Eng. J.,* 2021, **415**, 129031.

11 L. Chai, Z. Hu, X. Wang, Y. Xu, L. Zhang, T. T. Li, Y. Hu, J. Qian and S. Huang, *Adv. Sci.,* 2020, **7**, 1903195.

12 S. M. Kang, M. Kim, J. B. Lee and S. Xu, *Nanoscale,* 2021, **13**, 12854-12864.